Materials Advances

PAPER

Check for updates

From an insulating Zn-porphyrin metallacage to electrically conducting inclusion complexes featuring extended π-donor/acceptor stacks

Evan Thibodeaux, (ID) Paola A. Benavides, (ID) Ellis Barger, Rakesh Sachdeva and Sourav Saha (ID) *

π-Donor/Acceptor charge-transfer (CT) interactions between redox-complementary π-systems often give rise to non-native optical and electronic properties that are beneficial for modern electronics and energy technologies. However, the formation of extended supramolecular π-donor/acceptor stacks capable of long-range charge transport requires ingenious design strategies that can help reinforce otherwise weak π-donor/acceptor noncovalent interactions. Herein, we demonstrate that a large tetragonal prismatic metal–organic cage ($MOC2^{8+}$) having two parallel π-donor tetrakis(4-carboxyphenyl)-Zn-porphyrin (ZnTCPP) faces located ∼14 Å apart can accommodate up to three redox-complementary planar aromatic guests (either three π-acceptor guests or two π-acceptors surrounding one π-donor guest) between the ZnTCPP faces, forming extended π-donor/acceptor stacks. While empty $MOC2^{8+}$ behaves as an insulator due to the lack of charge delocalization across its large cavity, its inclusion complexes saturated with π-acidic hexaazatriphenylene hexacarbonitrile (HATHCN) and hexacyanotriphenylene (HCTP) displayed noticeably higher electrical conductivity (8.7×10^{-6} and 1.3×10^{-6} S m^{-1}, respectively) owing to more facile charge transport through the π-donor/acceptor stacks composed of the π-acidic guests intercalated between the ZnTCPP faces. Thus, this work demonstrates that tetragonal prismatic metallacages with two parallel electroactive faces can facilitate the creation of extended π-donor/acceptor stacks by encapsulating redox-complementary planar guests, which in turn facilitates through-space charge delocalization, generating non-native electrical conductivity.

Introduction

The facile charge delocalization capability of π-donor/acceptor (π-D/A) arrays[1–12] often creates fascinating electronic and optical properties that can help advance modern electronics, energy, and display technologies. Therefore, ever since the discovery of metallic conducting tetrathiafulvalene/tetracyanoquinodimethane (TTF/TCNQ) arrays decades ago,[2,6,7] π-donor/acceptor arrays have been drawing increasing attention thanks to their diverse light-harvesting, electrochromic, photochromic, thermochromic, and conducting properties.[13–28] While strong π-donor and acceptor pairs like TTF and TCNQ, which readily undergo formal intermolecular electron transfer generating radical ion pairs form parallel homomeric π-donor and acceptor columns that display metallic conductivity, weaker π-donor and acceptor molecules, which participate in charge-transfer (CT) and electrostatic interactions, typically form cofacially

π-stacked heterodimer and sandwich-type trimer complexes that behave more like semiconductors.[11,12,29] However, since the π-donor/acceptor CT interactions are relatively weak, to construct extended π-donor/acceptor stacks that can foster long-range charge delocalization, the π-donor and acceptor units must be connected by covalent linkers,[1,30–32] hydrogen bonds,[33–35] metal coordination,[36,37] or amphiphilic pendants.[38–43] These structural reinforcement measures, however, require covalent modifications of the π-donor and acceptor units, which could alter their intrinsic electronic properties and the nature of interactions, underscoring the need for less disruptive supramolecular approaches to assemble extended π-donor/acceptor stacks.

One such supramolecular assembly strategy involves the formation of inclusion complexes of prismatic metallacages with two parallel π-donor or acceptor faces that can sandwich redox-complementary guest π-systems, creating extended π-donor/acceptor stacks confined to the cage cavity. For example, Fujita's elongated trigonal prismatic Pd(II)-metallacages having two parallel π-acidic 1,3,5-triazine faces can host multiple planar

Department of Chemistry, Clemson University, 211 S. Palmetto Blvd., Clemson, South Carolina 29634, USA. E-mail: souravs@clemson.edu

templating guests inside their cavities, creating extended π-donor/acceptor stacks,[44–51] whereas Ribas' tetragonal prismatic metallacages[52–59] with two π-electron rich tetrakis(4-carboxyphenyl)-metalloporphyrin (MTCPP, M = Pd, Zn) faces also allow intercalation of planar and spherical guests. The height of these metallacages defined by the length of the pillar ligands connecting the two opposite faces regulate the size, shape, electronic properties, number, and order of the intercalated guest π-systems, which in turn, define the length of the supramolecular π-donor/acceptor stacks and their charge delocalization capability.

Although the guest recognition properties of metallacages have been widely studied,[44–59] the guest-mediated charge transport capability and electronic conductivity of their inclusion complexes have been rarely explored. To this end, Fujita et al.[50] first demonstrated tunable electrical resistor/rectifier behaviors of inclusion complexes of a 1,3,5-triazine-based metallacage, whereas we have recently demonstrated[60] that intercalation of a highly π-acidic hexaazatriphenylene hexacarbonitrile (HATHCN) guest molecule between two π-donor ZnTCPP faces of a tetragonal prismatic metal–organic cage MOC1[8+] (height ~7.5 Å) created a ZnTCPP/HATHCN/ZnTCPP stack, which created electrical conductivity by facilitating charge delocalization. Furthermore, metal–organic frameworks (MOFs) containing extended π-donor/acceptor stacks of either mixed-valent ligands[61–63] or complementary ligands and intercalated guests[64–66] display electrical conductivity due to facile through-space charge delocalization. Although metallacages have been widely used for various guest encapsulation, separation, storage, and delivery purposes,[67] they have been rarely employed to create extended π-donor/acceptor stacks through complementary guest encapsulation that can promote long-range charge delocalization and generate electrical conductivity.

Encouraged by these promising developments, herein, we employed a larger metal–organic cage MOC2[8+] having two ZnTCPP faces located ~14 Å apart according to its previously reported single-crystal structure,[53,58,59] which can accommodate up to three planar aromatic guests (the typical π–π-distance is ~3.3–3.5 Å) between the two ZnTCPP faces (Fig. 1), thus forming extended π-donor/acceptor stacks that can promote long-range charge delocalization. ^{1}H NMR, UV-vis, ESI-MS, and electrochemical studies confirmed the formation of inclusion complexes of MOC2[8+] with π-acidic HATHCN and hexacyanotriphenylene (HCTP) and a π-donor hexamethoxytriphenylene (HMTP, only in the presence of 2 equiv. of HATHCN), while electrochemical impedance spectroscopy (EIS) revealed that the inclusion complexes containing stronger π-acidic HATHCN guests produced higher electrical conductivity than those containing weaker π-acidic HCTP guests. The MOC2[8+] inclusion complex saturated with HATHCN displayed noticeably higher electrical conductivity than that containing fewer intercalated HATHCN molecules, demonstrating that continuous π-donor/acceptor stacks are more effective through-space charge transport conduits than the isolated heterodimers.

Results and discussion

Envisioning that tetragonal prismatic metallacages with large interfacial distance between two opposite π-donor faces should allow intercalation of multiple planar π-acidic guests and create extended π-donor/acceptor stacks, we constructed MOC2[8+] by connecting two electron-rich ZnTCPP faces with four bis-Pd-hexaazamacrocycle clips containing 4,4′-biphenyl spacers following a modified literature protocol (Fig. 1, see SI for details).[61]
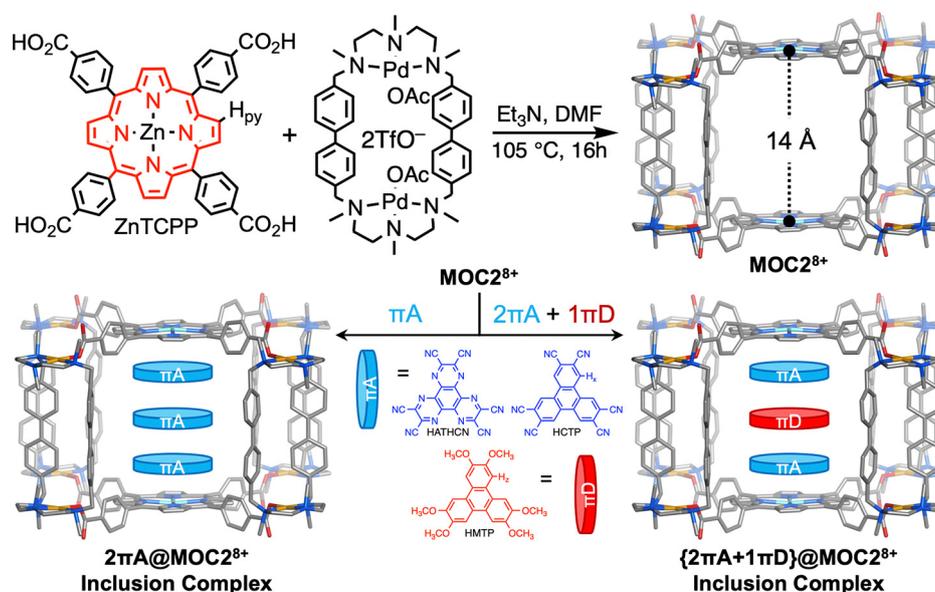

Fig. 1 Graphical representation of the synthesis of MOC2[8+] metallacages, followed by intercalation of multiple planar π-acceptor guest molecules between its two parallel π-donor ZnTCPP faces, leading to the formation of extended π-donor/acceptor stacks capable of long-range through-space charge delocalization.

The structure and composition of MOC2^{8+} were confirmed by ^{1}H, COSY and NOESY NMR spectroscopies and high-resolution ESI-MS analyses (Fig. S1–S4). According to its previously reported single-crystal and optimized structures,[58] the longer 4,4′-biphenyl spacers of bis-Pd-hexaazamacrocycle pillars positioned the two ZnTCPP faces of MOC2^{8+} *ca.* 14 Å apart. Given that the typical π–π-stacking distance is *ca.* 3.5 Å, this interfacial distance is ideal for the intercalation of as many as three planar guest π-systems and the formation of extended π-donor/acceptor stacks. For this purpose, we employed two planar π-acceptors, HATHCN and HCTP, which have similar size and shape but markedly different π-acidity (LUMO = −4.6 and −3.7 eV, respectively) as

well as a planar π-donor HMTP (HOMO = −5.2 eV) in order to study the guest-induced optical and electronic properties of the resulting inclusion complexes.

First, ^{1}H NMR titration experiments (Fig. 2a and b) revealed that upon addition of π-acidic HATHCN and HCTP molecules into MOC2^{8+}, the H$_{py}$ signal (pyrrole protons) of ZnTCPP faces and H$_x$ signal of HCTP shifted up-field, indicating that these π-acceptor guests were intercalated between the π-donor ZnTCPP faces of the cage. During ^{1}H NMR titration of MOC2^{8+} with HATHCN, the H$_{py}$ signal of ZnTCPP faces shifted rapidly from 8.62 to 8.47 ppm in the presence of 2 equiv. of HATHCN and then slowly to 8.44 ppm as the HATHCN concentration
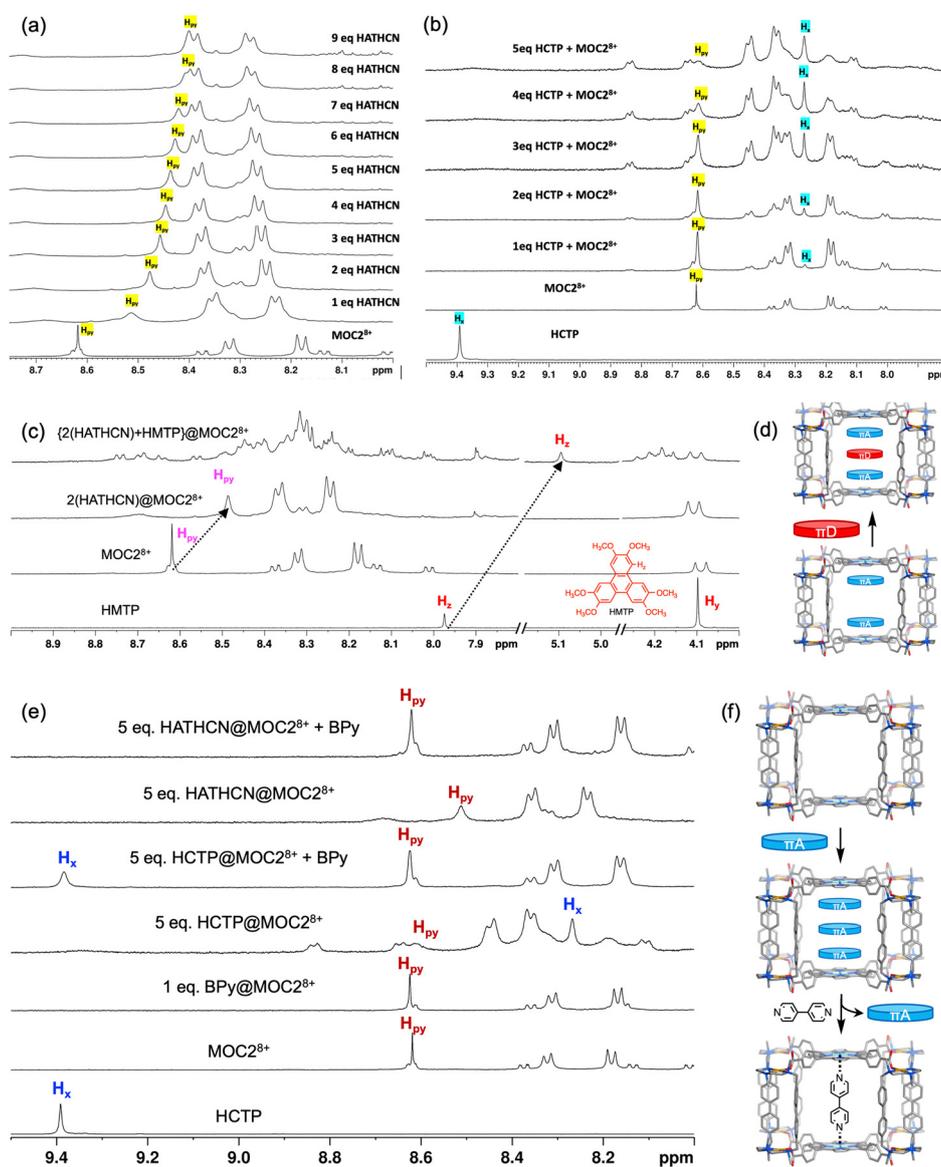
Fig. 2 Partial ^{1}H NMR (500 MHz, CD$_3$CN) titration of MOC2^{8+} with π-acidic (a) HATHCN and (b) HCTP guests show up-field shifts of ZnTCPP and π-acceptor signals upon guest intercalation. (c) Partial ^{1}H NMR (500 MHz, CD$_3$CN) spectra (from bottom to top) of free HMTP, empty MOC2^{8+}, 2(HATHCN)@MOC2^{8+}, and [{2(HATHCN) + HMTP}@MOC2]$^{8+}$ inclusion complexes show (d) the intercalation of HMTP between two pre-intercalated HATHCN molecules inside MOC2^{8+} cavity. (e) Partial ^{1}H NMR spectra (500 MHz, CD$_3$CN) and (f) a schematic representation depicting competitive displacement of intercalated π-acceptors (HATHCN and HCTP) from MOC2^{8+} upon axial coordination of Bpy with the ZnTCPP core indicated by the return of the ZnTCPP and the HCTP signals back to their original positions.

increased further. These observations suggested that the first two intercalated HATHCN molecules enjoyed strong π-donor/acceptor CT interaction with the ZnTCPP inner faces and thus caused the largest up-field shift. Given that the typical ZnTCPP/HATHCN distance is ∼3.5 Å, the interplanar distance between the first two intercalated HATHCN molecules adjacent to the inner ZnTCPP faces should be around 7 Å, which is sufficient for the intercalation of a third HATHCN molecule at higher guest concentrations. However, the third HATHCN molecule sandwiched between the other two intercalated HATHCN guests would exert negligible shielding effect on the ZnTCPP faces of MOC2^{8+}, which caused only modest up-field shift of H_{py} signal compared to the first two HATHCN molecules.

Since the shielding of intercalated HATHCN molecules inside MOC2^{8+} could not be probed by ^{1}H NMR spectroscopy due to the absence of H-atom on this π-acceptor, an isostructural, albeit a weaker, π-acidic HCTP guest was introduced to probe this phenomenon. Upon addition of a weaker π-acceptor HCTP to MOC2^{8+}, the H_x signal of HCTP shifted noticeably upfield (from 9.39 to 8.26 ppm) but up-field shift of the H_{py} signal of ZnTCPP faces was more modest (Fig. 2b) compared to that caused by the stronger π-acidic HATHCN due to weaker ZnTCPP/HCTP CT interaction. The NOESY NMR study revealed through-space coupling between the HCTP (H_x) and ZnTCPP (H_{py}) core protons (Fig. S3), further confirming guest intercalation. Interestingly, the intercalation of HCTP molecules inside the larger MOC2^{8+} cage caused much smaller up-field shift of its H_x ($\Delta\delta$ = 1.13 ppm) and ZnTCPP H_{py} peaks than its intercalation into smaller MOC1^{8+} ($\Delta\delta$ = 3.78 ppm) with a smaller cavity (height ∼7.5 Å).[60] This happened possibly because in larger MOC2^{8+}, each intercalated π-acceptor molecule interacts only with one ZnTCPP face, whereas in smaller MOC1^{8+}, the intercalated π-acceptor guest was tightly sandwiched between two π-donor ZnTCPP faces, interacting with both simultaneously, which caused a greater shielding.

We further envisioned that if a planar π-donor guest intercalated between two pre-intercalated HATHCN molecules bound to the inner ZnTCPP faces of the cage, it would help create an extended alternating π-donor/acceptor/donor′/acceptor/donor stack. To probe this possibility, we added 1 equiv. of a π-donor HMTP into a preformed 2(HATHCN)@MOC2^{8+} inclusion complex containing two intercalated HATHCN molecules bound to the inner ZnTCPP faces of the cage (MOC2^{8+} + 2 equiv. of HATHCN). This led to a dramatic upfield shift of the HMTP signals (H_z shifted from 7.97 to 5.09 ppm and H_y from 4.09 ppm to deeper into the aliphatic region), indicating that HMTP became sandwiched between two pre-intercalated π-acidic HATHCN molecules bound to the inner ZnTCPP faces of MOC2^{8+} (Fig. 2c and d). In a control experiment, the addition of HMTP to empty MOC2^{8+} did not cause any shift of the ZnTCPP (H_{py}) HMTP (H_y and H_z) signals, indicating that it did not enter into the empty cage due to the lack of electronic complementarity.

Next, we investigated competitive displacement of the intercalated guests from the MOC2^{8+} cavity upon axial coordination of a linear 4,4′-bipyridine (BPy) ligand, which can bridge the

inner faces of two ZnTCPP units (Fig. 2e and f).[55] Upon addition of 1 equiv. of BPy into MOC2^{8+} inclusion complexes containing intercalated HATHCN and HCTP guests, the α-Hs and β-Hs of BPy became extremely broad and almost disappeared, a tell-tale sign of axial coordination of BPy with ZnTCPP,[55] while the ZnTCPP (H_{py}) and π-acceptor (H_x) signals returned to their original positions, confirming the release of intercalated π-acceptors from the MOC2^{8+} cavity upon axial coordination of BPy. In addition, DOSY NMR studies (Fig. S4) revealed that both empty MOC2^{8+} and 1:1 BPy@MOC2^{8+} complex containing axially coordinated BPy ligands have essentially the same diffusion coefficients (D = 2.84 × 10^{-10} and 2.84 × 10^{-10} m^2 s^{-1}, respectively) and hydrodynamic radii (r_H = 21.98 and 22.23 Å, respectively). These results indicated that BPy intramolecularly bridged the two ZnTCPP faces of MOC28+ and ruled out its coordination with the outer ZnTCPP faces (this would have produced coordination polymers with much lower diffusion coefficients and larger hydrodynamic radius, which was not observed). This observation was consistent with Ribas' study showing that 4,4′-BPy axially coordinated with the inner ZnTCPP faces of MOC2^{8+}.[55] Furthermore, upon addition of 2 equiv. of HATHCN to 1:1 BPy@MOC2^{8+} complex containing internally coordinated BPy guest, the ZnTCPP H_{py} signal did not shift upfield (Fig. S5), suggesting that the π-acceptor did not bind to the outer ZnTCPP faces when an internally coordinated BPy molecule already occupied the MOC2^{8+} cavity. Taken together, these results unequivocally confirmed that the π-acceptor guests were only sandwiched between the two ZnTCPP faces of MOC2^{8+} and released upon internal axial coordination of BPy with the inner faces of ZnTCPP.

The inclusion complexes of MOC2^{8+} containing multiple π-acceptor guests were also detected by high-resolution ESI-MS analysis (Fig. 3a,b and Fig. S6–S9), which revealed the characteristic m/z signals of 1:2 host:guest complexes: [2(HATHCN)@MOC2·4BArF$_4$]$^{4+}$ (2339.6578), [2(HATHCN)@MOC2·3BArF$_4$]$^{5+}$ (1698.9133), [2(HATHCN)@MOC2·2BArF$_4$]$^{6+}$ (1271.9177), [2(HCTP)@MOC2·4BArF$_4$]$^{4+}$ (2337.1712), [2(HCTP)@MOC2·3BArF$_4$]$^{5+}$ (1697.1252), and [2(HCTP)@MOC2·2BArF$_4$]$^{6+}$ (1270.2607). In addition, the m/z signals corresponding to 1:1 host:guest complexes [[HATHCN)@MOC2·4 BArF$_4$]$^{4+}$ (2243.6488), [(HATHCN)@MOC2·3BArF$_4$]$^{5+}$ (1622.3067), [(HATHCN)@MOC2·2BArF$_4$]$^{6+}$ (1208.0781), [(HCTP)@MOC2·4BArF$_4$]$^{4+}$ (2242.4045), [(HCTP)@MOC2·3BArF$_4$]$^{5+}$ (1621.5116), and [(HCTP)@MOC2·2BArF$_4$]$^{6+}$ (1207.4164), as well as the empty cage [MOC2·4BArF$_4$]$^{4+}$ (2148.1394), [MOC2·3BArF$_4$]$^{5+}$ (1545.6985), and [MOC2·2BArF$_4$]$^{6+}$ (1144.4054) were also observed, suggesting that the intercalated π-acidic guests were released from the MOC2^{8+} cavity under the ionization conditions. Although MOC2^{8+} can, in principle, accommodate up to three planar π-acceptor molecules inside its large cavity (height ≈ 14 Å), no signals corresponding to 1:3 host:guest inclusion complexes were observed, possibly because the weakly bound third π-acceptor guest sandwiched between other two intercalated π-acceptors adjacent to the ZnTCPP inner faces was easily released from the cage, leaving the 1:2 host:guest complexes as the largest detectable species under electrospray ionization conditions. Nevertheless, the ESI-MS analysis also
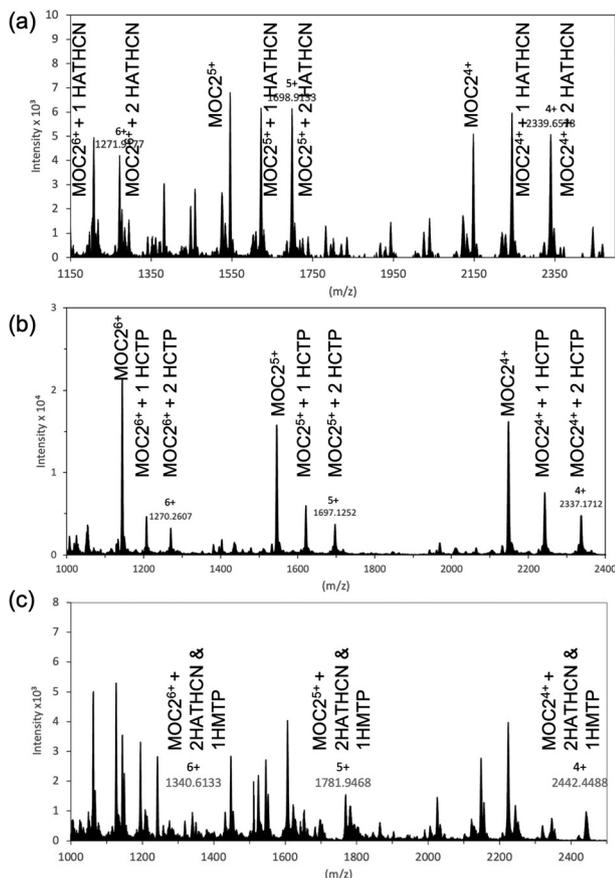
Fig. 3 ESI-MS analysis shows the characteristic m/z signals of MOC2^{8+} inclusion complexes containing intercalated (a) HATHCN, (b) HCTP, and (c) HATHCN and HMTP guests. The isotope distribution patterns are shown in Fig. S4–S7.

revealed (Fig. 3c) MOC2^{8+} inclusion complex containing two π-acidic HATHCN guests and one π-donor HMTP guest: [{2(HATHCN) + HMTP}@MOC2·4BArF$_4$]$^{4+}$ (2442.4488), [{2(HATHCN) + HMTP}@MOC2·3BArF$_4$]$^{5+}$ (1781.9468), [{2(HATHCN) + HMTP}@MOC2·2BArF$_4$]$^{6+}$ (1340.6133), confirming that it can accommodate up to three planar guests. In this case, the stronger HATHCN/HMTP/HATHCN charge-transfer interaction helped the π-donor HMTP guest sandwiched between two intercalated π-acceptor HATHCN molecules remain inside the cage, enabling its detection.

The UV-Vis titration of MOC2^{8+} with the stronger π-acceptor HATHCN (Fig. 4) caused significant quenching of ZnTCPP Soret and Q-bands and an emergence of a characteristic broad CT band appeared at 700 nm. The trend of HATHCN concentration-dependent quenching of ZnTCPP Soret band fits quite well with a 1:2 host:guest binding model (Fig. 4a, inset),[60] revealing the binding constants of $K_1 = 3.36 \times 10^4$ M^{-1}, $K_2 = 1.95 \times 10^3$ M^{-1}, and $K = K_1 \cdot K_2 = 6.55 \times 10^7$ M^{-2} (MeNO$_2$, 295 K). Although MOC2^{8+} can technically host up to three planar π-acidic guest molecules inside its large cavity, only two HATHCN molecules attached to the ZnTCPP inner faces were involved in π-donor/acceptor CT interaction, causing these spectroscopic changes, whereas the third HATHCN molecule sandwiched between the other two encapsulated HATHCN molecules did not have any significant impact on the ZnTCPP's optical properties. This explains why the HATHCN-induced UV-Vis absorption changes of MOC2^{8+} fit well with a 1:2 host:guest binding model and the 1:3 complex could not be detected. The weaker π-acidic HCTP did not cause any noticeable spectroscopic changes of MOC2^{8+}, further confirming that it was involved in a much weaker π-donor/acceptor CT interaction. It is worth noting that intercalation of a HMTP molecule between two pre-intercalated HATHCN guests inside MOC2^{8+} did not cause any noticeable spectroscopic changes, making it impossible to determine its association constant using UV-Vis spectroscopy.

Cyclic voltammetry studies (Fig. S10) revealed how the ZnTCPP/HATHCN CT interaction influenced their respective electronic properties, *i.e.*, redox potentials in the host–guest inclusion complexes. With increasing molar ratio of HATHCN (0–5 equiv. with respect to MOC2^{8+}), the first oxidation (anodic) peak of the ZnTCPP faces shifted gradually from +1130 to +1450 mV ($\Delta E_{ox} = +320$ mV, *vs.* $E_{Ag/AgCl}$), with the largest shift occurring in the presence 2 equiv. of HATHCN. This demonstrated that the intercalation of the first two HATHCN molecules involved in π-donor/acceptor CT interaction with the ZnTCPP faces exerted the greatest effect on the ZnTCPP oxidation. Similarly, upon addition of 2 equiv. of HATHCN to MOC2^{2+}, the first reduction (cathodic) peak of HATHCN shifted from −70 to −250 mV, ($\Delta E_{red} = -180$ mV, *vs.* $E_{Ag/AgCl}$), as the reduction of the intercalated HATHCN molecules became more difficult due to its CT interaction with π-donor ZnTCPP faces. In
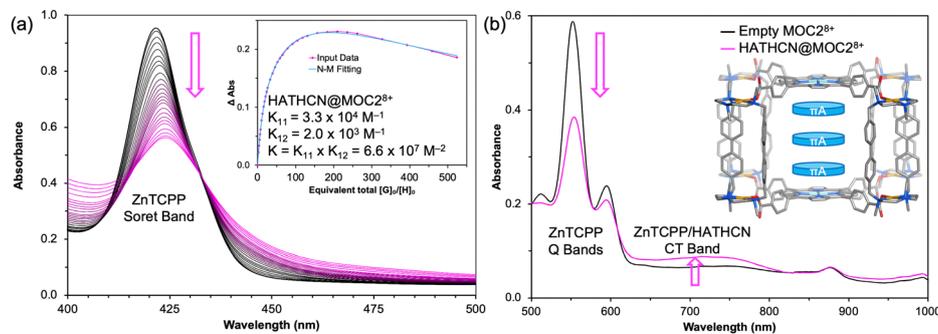

Fig. 4 (a) UV-Vis titration of MOC2^{8+} with HATHCN. Inset: Nelder-Mead fitting of HATHCN concentration-dependent quenching of ZnTCPP Soret band revealing a 1:2 host:guest binding model. (b) The UV-vis absorption spectrum of MOC2^{8+} inclusion complex saturated with HATHCN showed ZnTCPP/HATHCN CT interaction.
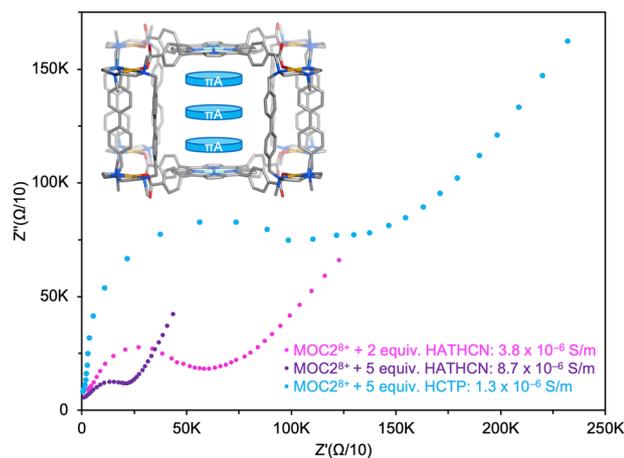
Paper

Fig. 5 The Nyquist plots of inclusion complexes of MOC2^{8+} containing HATHCN (2 and 5 equiv.) and HCTP (5 equiv.) show their respective electrical conductivity.

the presence of >2 equiv. of HATHCN, an additional cathodic peak appeared at *ca.* -100 mV, which was attributed to the reduction of the third HATHCN molecule sandwiched between the other two intercalated HATHCN molecules directly in contact with the ZnTCPP inner faces.

Finally, we measured the electrical conductivities of MOC2^{8+} and its inclusion complexes containing intercalated HATHCN and HCTP guests by electrochemical impedance spectroscopy (Fig. 5) using drop-cast films of these materials on interdigitated gold electrodes (Fig. S11). The Nyquist plots revealed that whereas the empty MOC2^{8+} cage behaved as an insulator with no measurable conductivity (*i.e.*, below the detection limit of the instrument, $<10^{-9}$ S m^{-1}) due to the lack of charge delocalization, its inclusion complexes enjoyed much smaller charge transfer resistance and higher electrical conductivity due to facile charge delocalization through the π-donor/acceptor stacks. The conductivity of MOC2^{8+} inclusion complex saturated with the stronger π-acidic HATHCN was almost 7 times higher than that saturated with weaker π-acidic HCTP (8.7×10^{-6} *vs.* 1.3×10^{-6} S m^{-1}, in the presence of 5 equiv. of respective guest), demonstrating that stronger π-donor/acceptor CT interaction created by the former enabled more efficient charge delocalization. However, at lower guest concentrations (2 equiv.), the unsaturated HATHCN@ MOC2^{8+} inclusion complex displayed a distinctly lower conductivity (3.8×10^{-6} S m^{-1}), while unsaturated HCTP@ MOC2^{8+} inclusion complex formed at lower guest concentration did not display any measurable conductivity. The guest concentration-dependent conductivity of MOC2^{8+} inclusion complexes further supported the possibility of intercalation of up to three planar π-acceptors at higher guest concentrations. These results also affirmed that continuous π-donor/acceptor stacks formed at higher guest concentrations were more efficient through-space charge transport conduits than the isolated or discontinuous π-donor/acceptor heterodimers formed at lower guest concentrations.

The π-acceptor guest-induced conductivity enhancement of MOC2^{8+} inclusion complexes, resulting from improved through-

space charge delocalization within the π-donor/acceptor stacks, was consistent with our previous study involving a smaller metallacage, MOC1^{8+},[60] which also exhibited a similar phenomenon upon π-acceptor guest intercalation, albeit to a smaller degree. Interestingly, although the smaller MOC1^{8+} displayed a noticeably higher intrinsic conductivity (2.5×10^{-6} S m^{-1})[60] than the larger empty MOC2^{8+} (*ca.* 8 *vs.* 14 Å interplanar distance between the two ZnTCPP faces),[58] the conductivity of the larger MOC2^{8+} inclusion complex saturated with HATHCN guests (up to three) was over 4 times higher than the 1:1 HATHCN@MOC1^{8+} inclusion complex (8.7×10^{-6} *vs.* 2.1×10^{-6} S m^{-1}),[60] possibly because the larger cage helped create more elongated π-donor/acceptor stacks capable of a longer-range charge delocalization than the smaller one.

Conclusion

The foregoing studies demonstrated the formation of inclusion complexes of a large tetragonal prismatic cage MOC2^{8+} having two π-donor ZnTCPP faces, which hosted up to three planar aromatic guests inside its large cavity creating extended π-donor/acceptor stacks that promoted through-space charge delocalization. The intercalation of stronger π-acidic HATHCN inside MOC2^{8+} generated more pronounced CT absorption band and caused more significant shifts in the redox potentials of both host and the guest than the weaker π-acidic HCTP guest due to stronger CT interaction of the former. Interestingly, although a π-donor HMTP molecule did not enter into empty MOC2^{8+} due to the lack of electronic complementarity, it became sandwiched between two pre-intercalated π-acidic HATHCN guests that were bound to the inner faces of ZnTCPP, forming an extended alternating D/A/D'/A/D stack. The empty MOC2^{8+} behaved as an electrical insulator, whereas its inclusion complexes saturated with intercalated HATHCN and HCTP guests displayed much higher conductivity (8.7×10^{-6} and 1.3×10^{-6} S m^{-1}, respectively), with the stronger π-acidic HATHCN generating a higher conductivity, demonstrating that stronger π-donor/acceptor CT interactions facilitated more efficient charge delocalization. Thus, our studies demonstrated that large prismatic metallacages having two parallel electroactive faces can serve as supramolecular containers to help assemble extended π-donor/π-acceptor stacks by hosting multiple redox-complementary planar guest molecules inside their cavities, delivering a simple strategy that can give the access to electrically conducting extended supramolecular π-donor/acceptor arrays and help advance molecular electronics.

Author contributions

The manuscript was written through contributions of all authors. All authors approved the final version of the manuscript.

Conflicts of interest

The authors declare no conflicts of interest.

Data availability

The data supporting this article have been included as part of the SI.

Additional experimental details, materials and methods, NMR, ESI-MS, and CV data (PDF). See DOI: **https://doi.org/10.1039/d5ma00653h**

Acknowledgements

References

1 R. S. Lokey and B. L. Iverson, *Nature*, 1995, **375**, 303–305.
2 J. Ferraris, D. O. Cowan, V. Walatka and J. H. Perlstein, *J. Am. Chem. Soc.*, 1973, **95**, 948–949.
3 M. Kumar, K. Venkata Rao and S. J. George, *Phys. Chem. Chem. Phys.*, 2013, **16**, 1300–1313.
4 J. K. Klosterman, M. Fujita and Y. Yamauchi, *Chem. Soc. Rev.*, 2009, **38**, 1714–1725.
5 A. Das and S. Ghosh, *Angew. Chem., Int. Ed.*, 2014, **53**, 2038–2054.
6 D. Jérome, *Chem. Rev.*, 2004, **104**, 5565–5591.
7 H. Alves, A. S. Molinari, H. Xie and A. F. Morpurgo, *Nat. Mater.*, 2008, **7**, 574–580.
8 W. Hayes and B. W. Greenland, *Adv. Polym. Sci.*, 2015, **268**, 143–166.
9 J. Zhang, W. Xu, P. Sheng, G. Zhao and D. Zhu, *Acc. Chem. Res.*, 2017, **50**, 1654–1662.
10 D. Venkataraman, S. Yurt, B. H. Venkatraman and N. Gavvalapalli, *J. Phys. Chem. Lett.*, 2010, **1**, 947–958.
11 T. Aoki, H. Sakai, K. Ohkubo, T. Sakanoue, T. Takenobu, S. Fukuzumi and T. Hasobe, *Chem. Sci.*, 2015, **6**, 1498–1509.
12 L. M. Klivansky, D. Hanifi, G. Koshkakaryan, D. R. Holycross, E. K. Gorski, Q. Wu, M. Chai and Y. Liu, *Chem. Sci.*, 2012, **3**, 2009–2014.
13 F. D'Souza, P. M. Smith, M. E. Zandler, A. L. McCarty, M. Itou, Y. Araki and O. Ito, *J. Am. Chem. Soc.*, 2004, **126**, 7898–7907.
14 E. Maligaspe, A. S. D. Sandanayaka, T. Hasobe, O. Ito and F. D'Souza, *J. Am. Chem. Soc.*, 2010, **132**, 8158–8164.
15 N. K. Subbaiyan, J. P. Hill, K. Ariga, S. Fukuzumi and F. D'souza, *Chem. Commun.*, 2011, **47**, 6003–6005.
16 D. K. Panda, F. S. Goodson, S. Ray, R. Lowell and S. Saha, *Chem. Commun.*, 2012, **48**, 8775–8777.
17 D. K. Panda, F. S. Goodson, S. Ray and S. Saha, *Chem. Commun.*, 2014, **50**, 5358–5360.
18 D. Gust, T. A. Moore and A. L. Moore, *Acc. Chem. Res.*, 2001, **34**, 40–48.
19 H. Imahori, *J. Phys. Chem. B*, 2004, **108**, 6130–6143.
20 S. Saha, E. Johansson, A. H. Flood, H. R. Tseng, J. I. Zink and J. F. Stoddart, *Chem. – Eur. J.*, 2005, **11**, 6846–6858.
21 J. B. Kelber, N. A. Panjwani, D. Wu, R. Gómez-Bombarelli, B. W. Lovett, J. J. L. Morton and H. L. Anderson, *Chem. Sci.*, 2015, **6**, 6468–6481.
22 X. Lv, W. Li, M. Ouyang, Y. Zhang, D. S. Wright and C. Zhang, *J. Mater. Chem. C*, 2017, **5**, 12–28.
23 J. J. Huang, H. A. Lin, C. Chen, P. W. Tang and S. C. Luo, *J. Mater. Chem. C*, 2021, **9**, 7919–7927.
24 P. M. Alvey, J. J. Reczek, V. Lynch and B. L. Iverson, *J. Org. Chem.*, 2010, **75**, 7682–7690.
25 C. Peebles, C. D. Wight and B. L. Iverson, *J. Mater. Chem. C*, 2015, **3**, 12156–12163.
26 T. Wang, Z. Hu, X. Nie, L. Huang, M. Hui, X. Sun and G. Zhang, *Nat. Commun.*, 2021, **12**(1364), 1–9.
27 S. Tayi, A. K. Shveyd, A. C. H. Sue, J. M. Szarko, B. S. Rolczynski, D. Cao, T. J. Kennedy, A. A. Sarjeant, C. L. Stern, W. F. Paxton, D. Wu, S. K. Dey, A. C. Fahrenbach, J. R. Guest, H. Mohseni, L. X. Chen, K. L. Wang, J. F. Stoddart and S. I. Stupp, *Nature*, 2012, **488**, 485–489.
28 S. K. Park, S. Varghese, J. H. Kim, S. J. Yoon, O. K. Kwon, B. K. An, J. Gierschner and S. Y. Park, *J. Am. Chem. Soc.*, 2013, **135**, 4757–4764.
29 P. A. Benavides, M. A. Gordillo, A. Yadav, M. A. Joaqui-Joaqui and S. Saha, *Chem. Sci.*, 2022, **13**, 4070–4081.
30 G. J. Gabriel and B. L. Iverson, *J. Am. Chem. Soc.*, 2002, **124**, 15174–15175.
31 M. Wolffs, N. Delsuc, D. Veldman, N. V. Anh, R. M. Williams, S. C. J. Meskers, R. A. J. Janssen, I. Huc and A. P. H. J. Schenning, *J. Am. Chem. Soc.*, 2009, **131**, 4819–4829.
32 D. Yuan, M. A. Awais, V. Sharapov, X. Liu, A. Neshchadin, W. Chen, M. Bera and L. Yu, *Chem. Sci.*, 2020, **11**, 11315–11321.
33 P. Mukhopadhyay, Y. Iwashita, M. Shirakawa, S. Kawano, N. Fujita and S. Shinkai, *Angew. Chem., Int. Ed.*, 2006, **45**, 1592–1595.
34 M. R. Molla and S. Ghosh, *Chem. – Eur. J.*, 2012, **18**, 9860–9869.
35 A. Mukherjee, S. Barman, A. Ghosh, A. Datta, A. Datta and S. Ghosh, *Angew. Chem., Int. Ed.*, 2022, **61**, e202203817.
36 S. Ghosh and S. Ramakrishnan, *Angew. Chem., Int. Ed.*, 2004, **116**, 3326–3330.
37 S. Ghosh and S. Ramakrishnan, *Macromolecules*, 2005, **38**, 676–686.
38 C. Wang, Z. Wang and X. Zhang, *Acc. Chem. Res.*, 2012, **45**, 608–618.
39 C. A. Sagade, K. V. Rao, U. Mogera, S. G. George, A. Datta and G. U. Kulkarni, *Adv. Mater.*, 2013, **25**, 559–564.
40 C. A. Sagade, K. V. Rao, S. G. George, A. Datta and G. U. Kulkarni, *Chem. Commun.*, 2013, **49**, 5847–5849.
41 K. V. Rao and S. G. George, *Chem. Eur. J.*, 2012, **18**, 14286–14291.
42 K. Liu, C. Wang, Z. Li and X. Zhang, *Angew. Chem.*, 2011, **123**, 5054–5058.
43 C. Wang, S. Yin, S. Chen, H. Xu, Z. Wang and X. Zhang, *Angew. Chem., Int. Ed.*, 2008, **47**, 9049–9052.
44 K. Kumazawa, K. Biradha, T. Kusukawa, T. Okano and M. Fujita, *Angew. Chem., Int. Ed.*, 2003, **42**, 3909–3913.

45 M. Yoshizawa, J. Nakagawa, K. Kumazawa, M. Nagao, M. Kawano, T. Ozeki and M. Fujita, *Angew. Chem., Int. Ed.*, 2005, **44**, 1810–1813.

46 M. Yoshizawa, K. Kumazawa and M. Fujita, *J. Am. Chem. Soc.*, 2005, **127**, 13456–13457.

47 K. Ono, M. Yoshizawa, T. Kato, K. Watanabe and M. Fujita, *Angew. Chem., Int. Ed.*, 2007, **46**, 1803–1806.

48 Y. Yamauchi, M. Yoshizawa, M. Akita and M. Fujita, *J. Am. Chem. Soc.*, 2010, **132**, 960–966.

49 T. Murase, K. Otsuka and M. Fujita, *J. Am. Chem. Soc.*, 2010, **132**, 7864–7865.

50 S. Fujii, T. Tada, Y. Komoto, T. Osuga, T. Murase, M. Fujita and M. Kiguchi, *J. Am. Chem. Soc.*, 2015, **137**, 5939–5947.

51 M. Iwane, T. Tada, T. Osuga, T. Murase, M. Fujita, T. Nishino, M. Kiguchi and S. Fujii, *Chem. Commun.*, 2018, **54**, 12443–12446.

52 C. García-Simón, M. García-Borràs, L. Gómez, I. García-Bosch, S. Osuna, M. Swart, J. M. Luis, C. Rovira, M. Almeida, I. Imaz, D. Maspoch, M. Costas and X. Ribas, *Chem. – Eur. J.*, 2013, **19**, 1445–1456.

53 C. García-Simón, M. García-Borràs, L. Gómez, T. Parella, S. Osuna, J. Juanhuix, I. Imaz, D. Maspoch, M. Costas and X. Ribas, *Nat. Commun.*, 2014, **5**, 5557.

54 C. Colomban, G. Szalóki, M. Allain, L. Gómez, S. Goeb, M. Sallé, M. Costas and X. Ribas, *Chem. – Eur. J.*, 2017, **23**, 3016–3022.

55 C. Colomban, V. Martin-Diaconescu, T. Parella, S. Goeb, C. García-Simón, J. Lloret-Fillol, M. Costas and X. Ribas, *Inorg. Chem.*, 2018, **57**, 3529–3539.

56 C. Fuertes-Espinosa, A. Gómez-Torres, R. Morales-Martínez, A. Rodríguez-Fortea, C. García-Simón, F. Gándara, I. Imaz, J. Juanhuix, D. Maspoch, J. M. Poblet, L. Echegoyen and X. Ribas, *Angew. Chem., Int. Ed.*, 2018, **57**, 11294–11299.

57 C. Colomban, C. Fuertes-Espinosa, S. Goeb, M. Sallé, M. Costas, L. Blancafort and X. Ribas, *Chem. – Eur. J.*, 2018, **24**, 4371–4381.

58 C. García-Simón, A. Monferrer, M. García-Borràs, I. Imaz, D. Maspoch, M. Costas and X. Ribas, *Chem. Commun.*, 2019, **55**, 798–801.

59 E. Ubasart, O. Borodin, C. Fuertes-Espinosa, Y. Xu, C. García-Simón, L. Gómez, J. Juanhuix, F. Gándara, I. Imaz, D. Maspoch, M. V. Delius and X. Ribas, *Nat. Chem.*, 2021, **13**, 420–427.

60 P. A. Benavides, M. A. Gordillo, E. Thibodeaux, A. Yadav, E. Johnson, R. Sachdeva and S. Saha, *ACS Appl. Mater. Interfaces*, 2024, **16**, 1234–1242.

61 M. A. Gordillo, P. A. Benavides, D. K. Panda and S. Saha, *ACS Appl. Mater. Interfaces*, 2020, **12**, 12955–12961.

62 M. A. Gordillo, P. A. Benavides, K. Spalding and S. Saha, *Front. Chem*, 2021, **9**(792), 1–6.

63 S. Zhang, D. K. Panda, A. Yadav, W. Zhou and S. Saha, *Chem. Sci.*, 2021, **12**, 13379–13391.

64 Z. Guo, D. K. Panda, M. A. Gordillo, A. Khatun, H. Wu, W. Zhou and S. Saha, *ACS Appl. Mater. Interfaces*, 2017, **9**, 32413–32417.

65 A. Yadav, S. Zhang, P. A. Benavides, W. Zhou and S. Saha, *Angew. Chem., Int. Ed.*, 2023, e202303819.

66 Z. Guo, D. K. Panda, K. Maity, D. Lindsey, T. G. Parker, T. E. Albrecht-Schmitt, J. L. Barreda-Esparza, P. Xiong, W. Zhou and S. Saha, *J. Mater. Chem. C*, 2016, **4**, 894–899.

67 C. T. McTernan, J. A. Davies and J. R. Nitschke, *Chem. Rev.*, 2022, **122**, 10393–10437.